On the Design of Video-Bandwidth Electric Field Sensing Systems Using Dielectric $LiNbO_3$ Electro-Optic Sensors and Optical Delays as Signal Carriers

Celso Gutiérrez-Martínez, *Member, IEEE*, Joel Santos-Aguilar, and Adolfo Morales-Díaz

***Abstract*— As the measurement of wide-band (multi-megahertz) electric fields is often of practical interest in industrial and commercial environments, in this paper, a methodology of design and implementation of a wide-band electric field sensing scheme, using optical delays as information carriers is described. The scheme is based on a lithium niobate ($LiNbO_3$) birefringent optical waveguide that performs simultaneously as an optical retarder and as a dielectric (electrode-less) sensor. In this scheme, the $LiNbO_3$ sensor introduces an optical delay and simultaneously senses an on-air electric field and imprints it around an optical delay. At the receiver, the sensed electric field is detected when the sensor and demodulator are optically matched, i.e., when both introduce identical optical delays. An important aspect, when sensing electric fields using $LiNbO_3$ dielectric sensors, is that the optically sensed field is weaker than the external field by a factor given by the ratio of the permittivity of the surrounding dielectric media over the $LiNbO_3$ permittivity (boundary condition for normal electric fields). When the surrounding media is air, the optically sensed electric field is 35 times weaker than the external field, as described in this paper. Another practical issue is that a birefringent optical waveguide is highly sensitive to optical polarization variations. Such a sensitivity implies that the output dc component of the received light changes with time (dc-drift). The dc-drift performance of the proposed electric field sensing scheme is measured and reported in this paper. The dc-drift can be minimized using polarization-insensitive $LiNbO_3$ unbalanced Mach–Zehnder interferometers.**

***Index Terms*— Lithium niobate $LiNbO_3$, dielectric electro-optic sensors, wide-band electric field sensing, optical retarders.**

I. Introduction

SENSING and measurement of wide-band (Multi-MHz) electric fields are important subjects in industrial and commercial human activities. Static and dynamic electric fields are produced by human activities or natural sources.

Manuscript received December 20, 2012; accepted May 14, 2013. Date of publication May 30, 2013; date of current version September 25, 2013. This work was supported by the Mexican Consejo Nacional de Ciencia y Tecnología CONACYT under Grant 67305-AC-2006-52148. The associate editor coordinating the review of this paper and approving it for publication was Dr. Shoushun Chen.

C. Gutiérrez-Martínez and A. Morales-Diaz are with the Instituto Nacional de Astrofísica Optica y Electrónica, Puebla 72000, Mexico (e-mail: cgutz@inaoep.mx).

J. Santos-Aguilar is with the Centro de Investigación Científica y Educación Superior de Ensenada, Ensenada 22860, Mexico (e-mail: jaguilar@inaoep.mx).

Color versions of one or more of the figures in this paper are available online at http://ieeexplore.ieee.org.

Digital Object Identifier 10.1109/JSEN.2013.2265169

Electric fields are commonly measured by electric or electronic instruments that are limited in bandwidth (some KHz) and sensitivity. Different techniques and devices for the measurement of electric fields have been reported in the technical literature [1]–[6]. Electro-mechanical electric field sensors, working in frequencies up to 2 KHz, are commercially available [7], [8].

An alternative to band-limited electric or electronic meters is the use of optical techniques. Optical techniques, using electro-optic sensors and optical fibers, are inherently wide-band, highly sensitive and immune to electromagnetic interference. Several electric field sensing schemes, using electro-optic devices, have been reported up to date. Most of such schemes are based on integrated optics Lithium Niobate ($LiNbO_3$) crystals and waveguides as electric field sensors. Sensor devices, either using electrodes, or electrode-less, have been studied and integrated on different experimental schemes [9]–[15].

Dielectric sensors are well adapted to the measurement of wide-band and high intensity fields, ranging from some kV/m to hundreds of kV/m [16]–[19]. Most of electric field sensing schemes are based on Mach-Zehnder (MZ) optical interferometers. In such configurations, the sensed electric field modulates the optical intensity of monochromatic light that is being guided by the electro-optic crystal or waveguide.

As demonstrated previously, in an alternative approach among the optical techniques, electric fields can be sensed by $LiNbO_3$ electro-optical retarders. The basic principle of this approach is that the electric field modulates an optical delay, instead of the optical intensity. The modulated optical delay is transmitted to an optical receiver. To demodulate the sensed electric field, the optical demodulator must be a second retarder, optically matched to the sensor.

Work describing the basic operating principles of electric field sensing using optical delays has been previously reported, demonstrating the potential sensing of low-frequency electric fields (up to 20 KHz) [20], [21]. At the time of our previous papers, the frequency response in our experiments was limited by an available wide-area and low-frequency photodetector whose response was limited to some tens of kHz.

As complementary work in our laboratory, and mainly aiming to improve our previous results, in the perspective of implementing really wider-band sensing schemes (multi-MHz frequency range), a detailed design methodology for

such a purpose, is proposed in this paper. To achieve a wide-band response, additional work has been conducted, given that our laboratory was granted some funds to acquire some low-cost high-speed PIN and APD photodetectors (1 GHz bandwidth) and a commercial high-voltage video amplifier (LEYSOP 250 series-500 Vpp in a 0-7 MHz band [22]). Such a high voltage amplifier is a high-tech component we used to generate high-intensity electric fields for testing multi-MHz schemes. The availability of these additional components allowed us to design and implement a complete video-band sensing scheme. This new stage in our research work makes the difference related to our previous papers and allowed us reaching more attractive improved results. A new aspect, not considered in our previous published works, and emphasized here, is that this time we could analyze the relationship between the optically sensed electric field and the real external field outside of the dielectric $LiNbO_3$ waveguide. In this case, and given that the electrooptic waveguide is electrode-less, the sensed electric field obeys the boundary conditions between the sensing waveguide and the external dielectric media. When the surrounding media is air, the optically sensed electric field is 35 times weaker than the electric field in the air. This condition states a scale factor when measuring external electric fields by using an $LiNbO_3$ optical waveguide as dielectric sensor.

In the perspective of this paper, to design and implement a wide-band dielectric sensing scheme, using an optical delay as signal carrier, requires the following steps:

a) Defining and fixing the optical delays (equivalently, the optical path-differences) that can be practically implemented.
b) Optically matching the sensor and demodulator at the same optical delays.
c) Modeling the field intensities relationship over an air-$LiNbO_3$ interface.
d) Calculating and measuring the electro-optic transfer function.
e) Calculating and measuring the half-wave electric field as a reference of the linear regions
f) Implementing, testing and characterizing the wide-band sensing scheme.

Once the operating parameters are fixed and experimentally characterized, the sensing scheme is implemented and tested for detecting high intensity-video-bandwidth electric fields.

A very attractive feature of using optical retarders is that such a technique allows serial multiplexing of optical delays and, and from this fact, multi-point sensing arrays can be configured. Optical serial multiplexing seems a promising technique for studying distributed sensing arrays as several optical delays can be cascaded over a single optical channel [20]. These multiplexing techniques have been barely studied and represent a potential applied research domain.

The summary of this paper is described as follows: in section II, the optical delay modulation principle is briefly recalled. In section III, the electric field sensing basis and the optical transfer function are deduced. The optical transfer function is a critical response, as it determines the linear and non-linear operating regions of the sensing scheme. In section IV, the experimental characterizations of the optical delays of the sensor and demodulator, half-wave electric field and bandwidth are realized. Finally, in section V, the experimental wide-band sensing set-up is tested and the system performances are reported. DC-drift is measured and compared to the DC-drift on an unbalanced MZ electrooptic sensor.

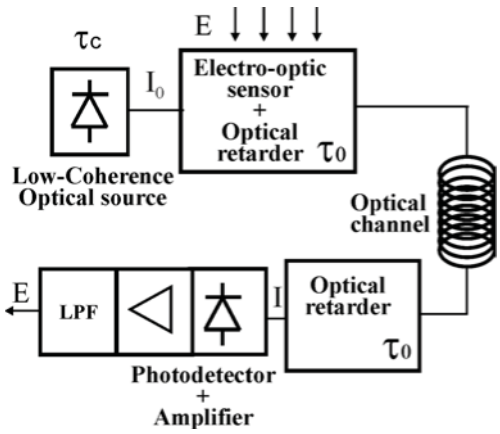

Fig. 1. An electric field sensing scheme using an optical delay as signal carrier.

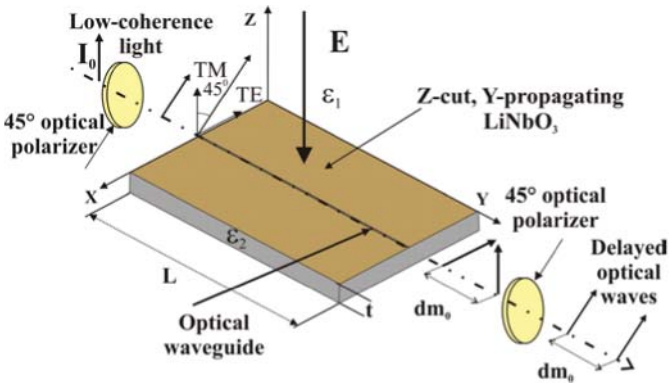

Fig. 2. An $LiNbO_3$ optical retarder-electric field sensor in a polarization interferometer configuration.

II. An Electric Field Sensing Scheme Based On Dielectric $LiNbO_3$ Optical Retarders

An electric field sensing system using an optical delay as a signal carrier, is depicted in fig. 1. In this scheme, the electro-optic sensor is an $LiNbO_3$ birefringent optical waveguide and the optical demodulator is a segment of birefringent polarization maintaining optical fiber (PMF).

The electro-optic sensor is an optical waveguide on a Z-cut, Y-propagating $LiNbO_3$ crystal of length L (mm) and thickness t (mm). The optical waveguide, acting as a polarization interferometer, as depicted in Fig. 2, will introduce a static optical delay τ_0 or its equivalent optical path-difference d_{m0}, when a low-coherence optical beam of constant power I_0, is linearly polarized at 45° and injected in the optical waveguide. Light is projected in TE and TM optical modes, which travel at different velocities through the optical waveguide, on depending of the ordinary n_o and extraordinary ne refractive

index. At the output of the optical waveguide, the delayed TE and TM modes will show a static optical path-difference, $dm0 = (no - ne)L$, which is designed to be longer than the coherence length of the optical source as to ensure no interference of the propagating modes.

The parameter d_{m0} can be modulated by the sensed electric field and transmitted through an optical channel.

At the receiver, an optical delay can be detected by measuring the autocorrelation of the transmitted light by using a second two-wave interferometer, in this case, a segment of PMF. The output of the second interferometer, when scanned in the optical path-difference axis d, shows a series interference fringe patterns, whose widths correspond to the coherence length of the optical source. The detailed description of the generation and detection of optical delays was presented in [20]. When two optical retarders are cascaded, the transmitted optical intensity, on depending on the optical path-difference d is given as

$$I(d) = \frac{1}{4} I_0 + \frac{I_0}{4} g(d) + \frac{I_0}{8} g(d - d_{m0}) + \frac{I_0}{8} g(d + d_{m0}) \quad (1)$$

I_0, as shown in fig. 2, is the constant optical power at the input of the first polarizer. The detected optical intensity depends on the optical autocorrelation of the received light.

$$g(d) = |g(d)| \cos\left(\frac{2\pi}{\lambda_0} d\right) \quad (2)$$

To recuperate a signal imprinted around $d = +d_{m0}$, the optical demodulator needs to be adjusted at the same optical path-difference, i.e. the sensor and receiver must be optically matched. Under such a condition, as $g(d_{m0}) = g(2\,d_{m0}) = 0$, the recovered optical intensity is

$$I(d) = \frac{1}{4} I_0 + \frac{I_0}{8} g(0) \quad (3)$$

Expression 3 corresponds to an interference fringe pattern, located around $d = +d_m 0$ and over an average optical power $1/4\, I_0$.

In the sensing scheme shown in figure 1, the optical demodulator is a segment of PMF, whose inherent birefringence is able to introduce an optical delay.

III. Electric Fields Relationship on an Air-Dielectric $LiNbO_3$ Interface

As the $LiNbO_3$ optical waveguide is used as a dielectric sensor, no electrodes are associated to the crystal and the external electric field is present in the dielectric media surrounding it, fig. 2. When an external electric field E is sensed by the electro-optic waveguide, the optically sensed field intensity Ez is determined by the boundary conditions between the dielectric media and the waveguide. The interface discontinuity is determined by the relative permittivity of both dielectrics (air, $\varepsilon_{r1} = 1$; $LiNbO_3$ crystal, $\varepsilon_{r2} = 35$). When the optically sensed electric field Ez is perpendicular to the crystal surface, the relationship between the field components E and Ez, is given as [23]

$$E_z = \frac{\varepsilon_{r1}}{\varepsilon_{r2}} E \quad (4)$$

According to (4), the sensed electric field Ez, is 35 times weaker than the electric field intensity in the air. Keeping in mind this relationship, the sensing system is modeled just considering the field Ez, inside the optical waveguide. Later, to know the real external field intensity, it will be necessary to scale the optically sensed electric field by 35 for finding the real external intensity. In this way, and coming-back to fig. 2, when an electric field $E_z(t)$ is sensed by the electro-optic retarder, it induces a dynamic variation of optical path-difference $\Delta d(t) = K \frac{\varepsilon_{r1}}{\varepsilon_{r2}} E(t)$ around $d = +dm0$. K is a proportionality constant. The sensed electric field Ez is oriented on the Z-axis of the $LiNbO_3$ crystal, interacting with the linear electro-optic coefficients r_{13} and r_{33}. Now, after expressions 2 and 3, for detecting the sensed field, the sensor and demodulator are cascaded and optically matched at $d = +d_{m0}$. Under such a condition

$$I(t) = \frac{I_0}{4} + \frac{I_0}{8} \cos\left[\frac{2\pi}{\lambda_0} \Delta d(t)\right] \quad (5)$$

As $\Delta d(t) = K \frac{\varepsilon_{r1}}{\varepsilon_{r2}} E(t)$ then $K = \frac{\lambda_0}{2 E_\pi}$. E_π is the half-wave electric field given as

$$E_\pi = \lambda_0 \Big/ \left(r_{33}\, {n_e}^3\, \Gamma_{TM} - r_{13}\, {n_o}^3\, \Gamma_{TE}\right) L_e \quad (6)$$

The half-wave electric field depends on the electro-optic parameters and on the interaction length L_e, between the electric and optical fields; Γ_{TE} and Γ_{TM} are the electric-optical overlapping coefficients; n_0, n_e are the optical ordinary and extraordinary refractive index, respectively.

By fine adjusting the optical demodulator at a static optical path-difference of $d = (d_{m0} - \frac{\lambda_0}{4})$, a linear detection of the imprinted electric field can be achieved. Under such a condition, the optical transfer function, given by eq. 5, becomes

$$I(t) = \frac{I_0}{4} + \frac{I_0}{8} sin\left[\pi \frac{\varepsilon_{r1}}{\varepsilon_{r2}} E(t) \Big/ E_\pi\right] \quad (7)$$

Even if, as stated by eq. 4, the sensed electric field varies linearly related to the external field E, at the receiver, the detected optical power varies as a sinusoidal function of E, as given by eq. 7. The optical half-wave electric field E_π is defined as the electric field intensity that switches the optical output in eq. 7, between its maximum and minimum values, $\frac{3I_0}{8}$ and $\frac{I_0}{8}$, respectively. A linear sensing process takes place in the linear region, around the quadrature points of the transfer function.

IV. Implementing Wide-Band Electric Field Sensing Operating Parameters

To experimentally implement a wide-band and optical-delay based electric filed sensing scheme, a minimum methodology was stated in the final paragraphs of the introduction section of this paper. In this way, the characterization and measurement of the main parameters of the sensing scheme are described in this section.

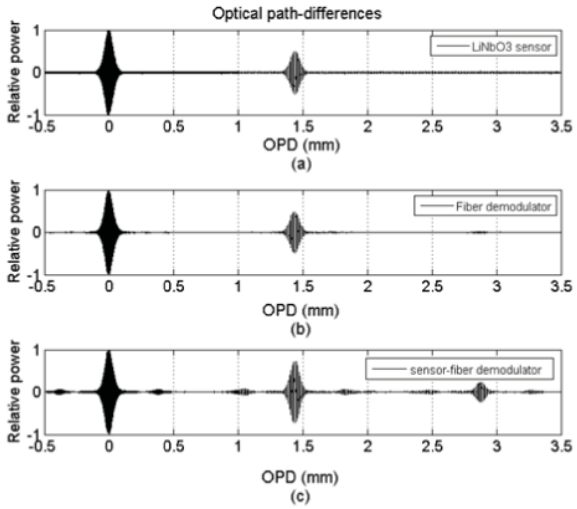

Fig. 3. Measured 1.45 mm optical path-differences: (a) sensor; (b) demodulator; and (c) matched sensor-demodulator.

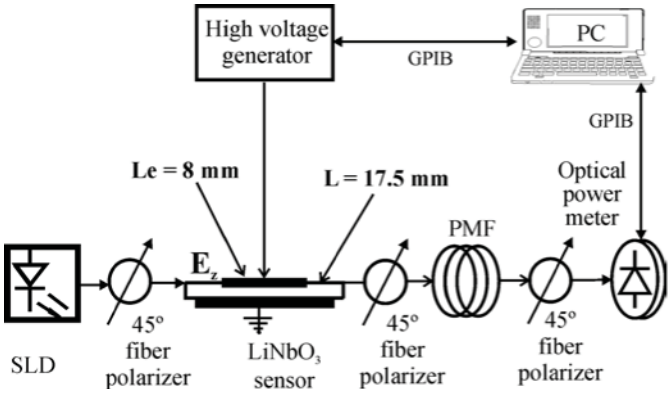

Fig. 4. Experimental set-up for measuring the optical transfer function of an optical delay-electric field sensing scheme.

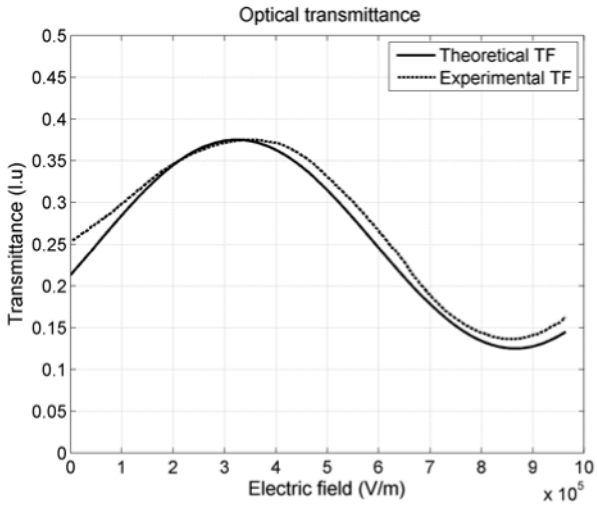

Fig. 5. Theoretical and experimental electro-optic transfer function of a $LiNbO_3$ waveguide.

A. Optical Path-Differences

To implement an electric field sensing scheme using optical delays, a main step to accomplish is the measurement of the optical path-differences on either, the electro-optic sensor and the optical demodulator. As explained in section II, the electric field sensor will introduce a static path-difference d_{m0}, which, at the same time, will be modulated by the sensed electric field. The transmitted optical delay will be demodulated at the receiver and the sensed electric field will be detected only when the sensor and demodulator are optically matched. As explained elsewhere [20], [21], optical delays can be measured by scanning Michelson interferometry, which allows the measurement of the interference fringe patterns around the introduced path-differences. In this work, the measured optical retarder/electro-optic sensor is a 17.5 mm-long, Z-cut, Y-propagating fiber-pigtailed $LiNbO_3$ optical waveguide. For such a waveguide, the theoretical static path-difference is $d_{m0} = 1.4525$ mm. The optical demodulator is a 4.61 m segment of PMF (3M, FS-CG-6121), which introduces the matching optical path-difference. The measured fringe patterns are depicted in fig. 3. Fig. 3(a) shows the measurement of d_{m0}, at 1.45 mm, for the $LiNbO_3$ waveguide. The fringe pattern around zero corresponds to the optical source, showing a coherence-length of about 80 μm. Fig. 3(b) shows the matched path-difference, as introduced by the PMF segment. Fig. 3(c) shows the superimposed fringe patterns, when the sensor and PMF demodulator are cascaded, thus demonstrating that both components are optically matched.

B. Half-Wave Electric Field of the Electro-Optic Sensor

The half-wave electric field sensor can be measured by using the set-up in fig. 4. For such a purpose, a DC electric field has been generated by using a set of parallel plates, which are driven by a high voltage-video generator [22]. In this case, the plates are 8 mm-long and in contact with the electrooptic crystal. The electric field is then directly sensed by the optical waveguide. A computer program for controlling the high voltage power supply and the optical power meter through a GPIB-interface, has been developed. The program sweeps a high voltage between the parallel plates in order to generate a testing DC electric field. The test field has been varied in a range of 0-950 kV/m for observing a cycle of eq. 7 and measuring the half-wave electric field.

Light coming from a super-luminiscent diode (SLD), is injected in the sensing optical waveguide. The optical waveguide introduces an optical path-difference d_{m_0}, which, at the same time, is modulated by the sensed electric field. The modulated optical signal is transmitted to the PMF, where optical demodulation takes place and the optical transfer function is automatically recorded. The optical transfer function for an electro-optic interaction length of 8 mm, is shown in fig. 5. In this figure, theoretical and experimental functions, are displayed.

The measured transfer function is in good agreement to the theoretical prediction given by eq. 6. The theoretical half-wave electric field E_π is 542.5 kV/m and the measured value is 493.5 kV/m.

The optical transfer function shows the different linear sensing ranges, on depending on the electric field intensities.

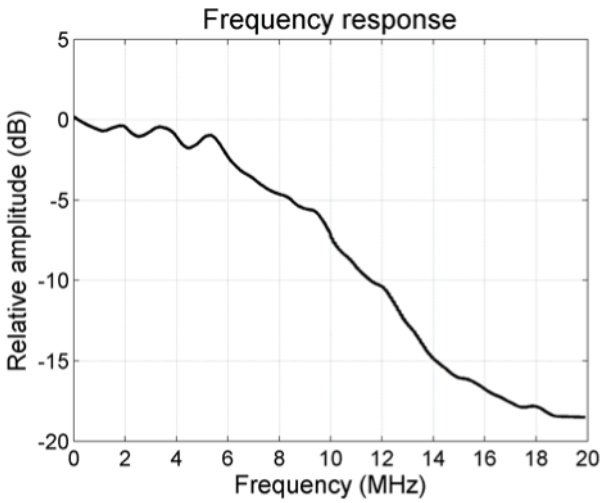

Fig. 6. Measured frequency response of the electric filed sensing scheme.

Linear ranges are between 0 and 200 kV/m and between 500 and 700 kV/m. From the graphs in fig. 5, it can be deduced that linear sensing is obtained when the sensor is biased at DC electric fields around 0 and 550 kV/m.

C. Frequency Response of the Electric Field Sensing Set-Up

The measured frequency response of the sensing scheme is illustrated in fig. 6. The 3-dB electrical bandwidth is around 6 MHz and is limited by the frequency response of the high voltage video amplifier used to generate a video-band electric field. This improved response is much higher to the audio-frequency band that was tested in our previous work [21]. Such a multi-MHz band was achieved as a high voltage-video amplifier was available in our laboratory. The inherent frequency response of $LiNbO_3$ sensors, when sensing an external electric field as generated by parallel plates, goes potentially up to 2 GHz, hence its use for sensing microwave electric fields is only limited by the frequency response of the photo-receiver and the processing electronics.

V. Testing the Video-Band Electric Field Sensing Scheme

To show the practical application of the implemented sensing scheme, based on optical delays, an experimental set-up was configured for sensing high-intensity multi-MHz electric fields, fig. 7. In fig. 8, the photograph of our laboratory experimental set-up is also shown. The scheme uses the fiber-pigtailed 17.5 mm-long $LiNbO_3$ electro-optic sensor (inset in fig. 8), which has been previously characterized as an optical retarder. The optical demodulator is a segment of 4.61m of PMF. The experimental set-up includes a SLD emitting at 1310 nm; a 10-MHz band photo-receiver and single mode optical fiber channel. The first linear region of transfer function in fig. 5, around 0 kV/m, has been used for sensing 0-7 MHz AC electric fields. The electric field is generated by applying a high AC voltage from the video amplifier to the parallel plates. To achieve a linear modulation, the electro-optic sensor was biased at a static electric field

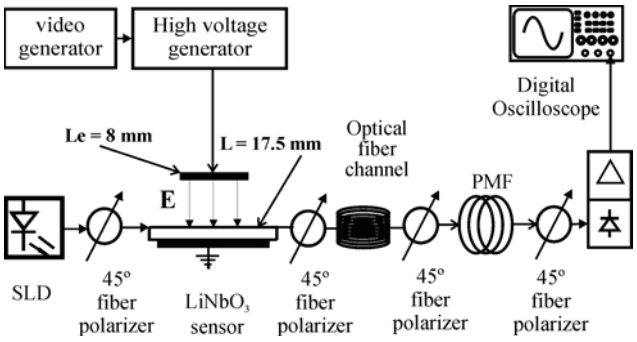

Fig. 7. Experimental wide-band electric field sensing set-up using an optical path-difference as information carrier.

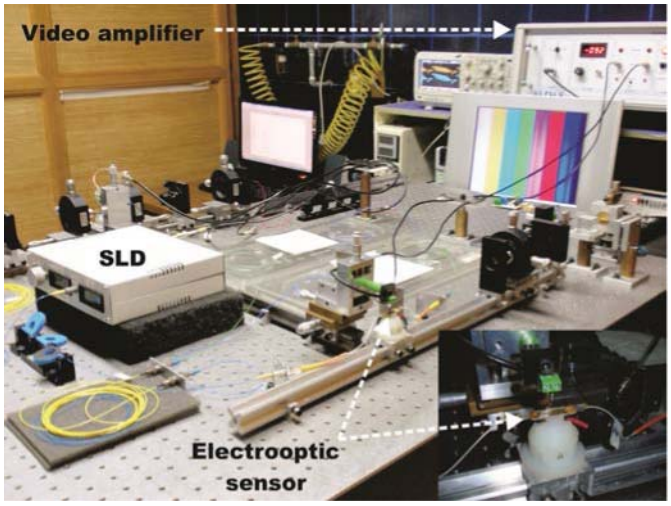

Fig. 8. The experimental optical delay-based electric field sensing set-up.

around 0 kV/m. The static electric field bias point is provided by the high-voltage video amplifier, whose output can fix an offset static DC voltage on the parallel plates. To test the sensing scheme, an AC electric field, ranging between $E_{pp} = 0$ kV_{pp}/m and $E_{pp} = 150$ kVpp/m, around 0 Kv/m on the electrooptic transfer function of fig. 5, was generated. This electric field range corresponds to the field sensed by the optical waveguide.

It is very convenient to remind that after eq. 3, the strength of the electric field in the air layer above the crystal surface is 35 times stronger than the measured by the optical waveguide.

Such a condition implies that the in-air sensed electric field ranges between 0-5.25 MVpp/m. On the sensing device, the effective electrical-optical interaction length is 8 mm. Such a length determines a sensing range going up to several MVpp/m.

The sensing range can be lowered by increasing the electrical-optical interaction length.

After optical transmission, a 10-MHz trans-impedance photo-receiver detected the optical signal, giving an AC voltage proportional to the sensed electric field.

The output voltage values, corresponding to a range of $0V_{pp}/m \leq E_{pp} \leq 5.25$ MV_{pp}/m, are displayed in figure 9. In this figure, the dots represent the measured output voltages. The linear fitting of the measured voltages is also shown. The linear relationship, $Vo = 0.0000007 * E_{pp} + 0.5077$, represents

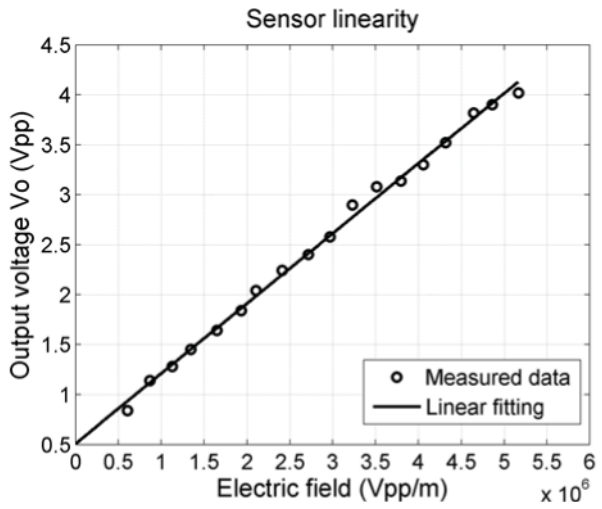

Fig. 9. The linear response of the sensing scheme in 0-5.25 MVpp/m range.

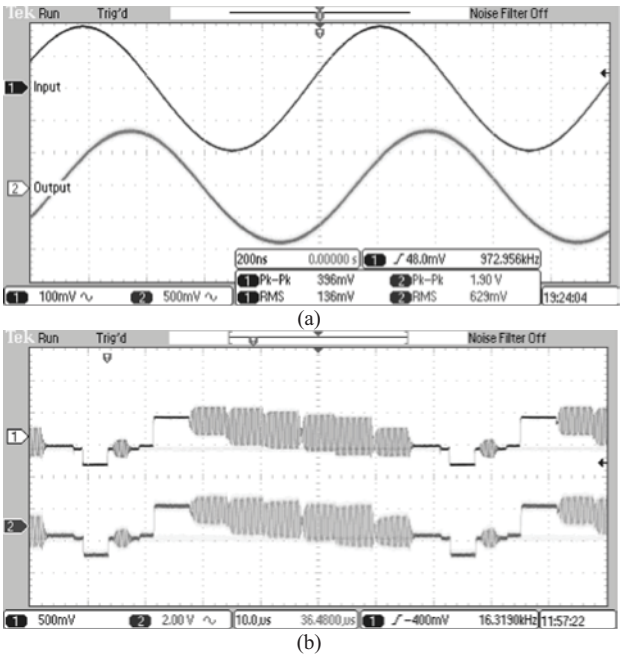

Fig. 10. (a) 1 MHz, 2.1 MVpp electric field. (b) Video electric field.

the calibration curve of the sensing scheme in the 0-5 MV_{pp}/m range. The measurement of a 1 MHz sinusoidal electric field of 2.1MV_{pp}/m (190mV_{pp} output signal) is shown in fig. 10(a). In fig. 10(b), the detection of a video electric field is also displayed. In these graphs, the upper waveform corresponds to the input voltage to the video amplifier; the lower waveform corresponds to the output voltage as delivered by the trans-impedance photo-receiver. The output noise has been measured and is limited to 0.0175Vrms. For an output voltage of 1.9V_{pp} (0.671 Vrms), the signal to noise ratio is better than 30 dB [24], [25]. The tested sensing scheme represents a promising technique as it shows a high-quality sensing-detection process including wide-band frequency response, high linearity and high signal to noise ratio.

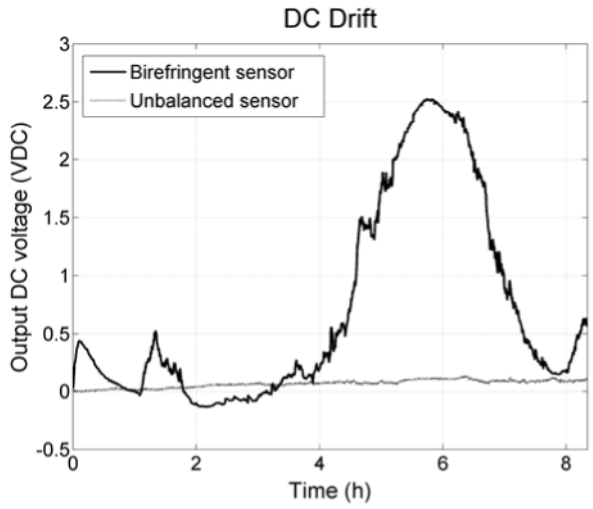

Fig. 11. DC-drift comparison.

VI. DC-Drift Stability on $LiNbO_3$ Dielectric Sensors

Birefringent $LiNbO_3$ optical waveguides, used as electric field sensors, show inherent DC-drift instability, as a result of the polarization sensitivity due to temperature variations. The DC-drift manifests as a mean DC voltage variation at the output of the electric field sensing scheme. The DC-drift of our electric field sensing scheme was measured and the performance is shown in figure 11. The DC-drift ranges between 0 and +2.5 VDC, in an 8 hours period. When using $LiNbO_3$ birefringent sensors, the compensation of the DC drift requires that the mean DC output voltage can be monitored and continuously adjusted, as to ensure a 0 VDC output at any time. This monitoring requires that light, at the output of the electrooptic sensor, be sampled and photodetected to give the DC-drift voltage. Such a voltage will be compared to a reference dc voltage. An error voltage will be generated in order to adjust the dc operating point as to maintain the dc static electric field at the quadrature point on the electrooptic transfer function. A potential solution of the DC-drift on birefringent electrooptic sensors is the use of polarization insensitive electrooptic devices. Such devices are optical unbalanced MZ interferometers, implemented on a X-cut, Z-propagating $LiNbO_3$. In this case, an optical delay can be introduced by a differential length of the interferometer arms and the device performs as a polarization insensitive sensor, as it does not exhibit birefringence. In the X and Y axes, the refractive index is the ordinary one(*n0*), hence, there is no birefringence and an optical delay can be introduced only by different path lengths. In the aim of a quantitative comparison, the DC-drift on an unbalanced MZ-interferometer has been measured and is also shown in figure 11. The unbalanced MZ interferometer shows minimum DC-drift when compared to the birefringent sensor response.

VII. Conclusion

In this paper, a multi-MHz electric field sensing scheme, based on an optical delay, has been reported. The operating

principle is based on the introduction of an optical path-difference, by a birefringent electro-optic $LiNbO_3$ waveguide, which, at the same time, acts as electric field sensor. The optical path-difference is modulated by the wide-band sensed electric field. The optical transfer function is a very important characteristic as it determines the linear and non-linear operating regions of the electro-optic sensor. In this work a 17.5-mm optical waveguide introduced an optical path-difference of 1.4525 mm, which acts as the optical carrier. The electric field-modulated optical carrier can only be demodulated by matching a second optical path-difference of 1.4525 mm.To show a practical application, the 17.5 mm sensor was integrated in a sensing scheme and AC electric fields, in a band up to 7 MHz, were successfully measured. The linear sensing of a 0-5.25 MVpp/m electric field range has been demonstrated. The scheme exhibits a high linear response when the sensor has been biased at around a 0 kV/m static electric field. The electric field sensing range was determined by the 8 mm electrical/optical interaction distance. The measurements show a high signal to noise ratio of around 30 dB.The optically detected electric field can be measured and the real external electric field is 35 times greater, as described in the paper. The DC-drift is a characteristic of a birefringent $LiNbO_3$ electrooptic sensor. To compensate for such an effect, a polarization-insensitive unbalanced $LiNbO_3$ MZ-interferometer, can be used to configure wide-band, optical delay-based electric field sensing scheme. Work is in progress in our laboratory to configure experimental schemes using polarization-insensitive electrooptic sensors.

ACKNOWLEDGMENT

The authors would like to thank the grant 67305-AC-2006-52148 from the Mexican Consejo Nacional de Ciencia y Tecnología (CONACYT), for supporting this work.

REFERENCES

[1] N. S. Nahman, M. Kanda, E. B. Larsen, and M. L. Crawford, "Methology for standard electromagnetic field measurements," *IEEE Trans. Instrum. Meas.*, vol. 34, no. 4, pp. 490–503, Dec. 1985.

[2] A. R. Johnston, H. Kirkham, and B. T. Eng, "DC electric field meter with fiber optic readout," *Rev. Sci. Instrum.*, vol. 57, no. 11, pp. 2746–2753, Nov. 1986.

[3] H. Kirkham, "Measuring electric fields from power lines: Part 1," *IEEE Instrum. Meas. Mag.*, vol. 9, no. 3, pp. 54–56, Jun. 2006.

[4] H. Kirkham, "Measurement of electric fields generated from alternating current," *IEEE Instrum. Meas. Mag.*, vol. 9, no. 5, pp. 58–61, Oct. 2006.

[5] H. Kirkham, "Dust devil and dust fountains: The measurement challenges," *IEEE Instrum. Meas. Mag.*, vol. 9, no. 6, pp. 48–52, Dec. 2006.

[6] C. J. Harland, T. D. Clark, and R. J. Prance, "Remote detection of human electroencephalograms using ultrahigh input impedance electric potential sensors," *Appl. Phys. Lett.*, vol. 81, no. 17, pp. 3284–3286, Oct. 2002.

[7] (2012, Aug.). *Electric Field Sensor*, Campbell Scientific Inc., Logan, UT, USA [Online]. Available: http://www.campbellsci.com/electric-fiels-sensor CS110

[8] (2012, Aug.). *Electric Field Mill Sensor EFS 1000 Series*, Mission Instruments Corporation, Tucson, AZ, USA [Online]. Available: http://www.missioninstruments.com/pages/products/efs1000.html

[9] N. A. F. Jaeger and L. Young, "High-voltage sensor employing an integrated optics Mach-Zehnder interferometer in conjuction with a capacitive divider," *IEEE J. Lightw. Technol.*, vol. 7, no. 2, pp. 229–235, Feb. 1989.

[10] T. Meier, C. Kostrzewa, K. Petermann, and B. Schuppert, "Integrated optical E-field probes with segmented electrodes," *IEEE J. Lightw. Technol.*, vol. 12, no. 8, pp. 1497–1503, Aug. 1994.

[11] Y.-S. Yim, S.-Y. Shin, W.-T. Shay, and C.-T. Lee, "Lithium niobate integrated-optic voltage sensor with variable sensing ranges," *Opt. Commun.*, vol. 152, nos. 4–6, pp. 225–228, Jul. 1998.

[12] Y.-K. Choi, M. Sanagi, and M. Nakajima, "Measurement of low frequency electric field using Ti:$LiNbO_3$ optical modulator," *IEE Proc. J. Optoelectron.*, vol. 140, no. 2, pp. 137–140, Apr. 1993.

[13] D. H. Naghski, J. T. Boyd, H. E. Jackson, S. Sriram, S. A. Kingsley, and J. Latess, "An integrated photonic Mach-Zehnder interferometer with no-electrodes for sensing electric fields," *IEEE J. Lightw. Technol.*, vol. 12, no. 6, pp. 1092–1097, Jun. 1994.

[14] Z. Fuwen, C. Fushen, and Q. Kun, "An integrated electro-optic E-field sensor with segmented electrodes," *Microw. Opt. Technol. Lett.*, vol. 40, no. 4, pp. 302–305, Feb. 2004.

[15] T.-H. Lee, F.-T. Hwang, W.-T. Shay, and C.-T. Lee, "Electromagnetic field sensor using Mach-Zehnder waveguide modulator," *Microw. Opt. Technol. Lett.*, vol. 48, no. 9, pp. 1897–1899, Sep. 2006.

[16] K. Hidaka and H. Fujita, "A new method of electric field measurements in corona discharge using Pockels device," *J. App. Phys.*, vol. 53, no. 9, pp. 5999–6003, Sep. 1982.

[17] Y. J. Rao, H. Gnewuch, C. N. Pannell, and D. A. Jackson, "Electro-optic electric field sensor based on periodically poled $LiNbO_3$," *Electron. Lett.*, vol. 35, no. 7, pp. 596–597, Apr. 1999.

[18] V. N. Filippov, A. N. Starodumov, Y. O. Barmenkov, and V. V. Makarov, "Fiber-optic voltage sensor based on a $Bi_{12}TiO_{20}$ crystal," *App. Opt.*, vol. 39, no. 9, pp. 1389–1393, Mar. 2000.

[19] F. Cecelja, M. Bordovsky, and W. Balachandran, "Lithium niobate sensor for measurement of DC electric fields," *IEEE Trans. Instrum. Meas.*, vol. 50, no. 2, pp. 465–469, Apr. 2001.

[20] C. Gutierrez-Martínez, "Electric field sensing schemes using low-coherence light and $LiNbO_3$ electrooptical retarders," in *Optical Fibre, New Developments*, C. Lethien, Ed. Vukovar, Croatia: InTeh, Dec. 2009, ch. 6.

[21] C. Gutiérrez-Martínez and J. S. Aguilar, "Electric field sensing scheme based on matched $LiNbO_3$ electro-optic retarders," *IEEE Trans. Instrum. Meas.*, vol. 57, no. 7, pp. 1362–1368, Jul. 2008.

[22] (2012, Nov.). *250 Series High Voltage Video Amplifier*, Leysop Ltd., Essex, U.K. [Online]. Available: http://www.leysop.com/m250.htm

[23] C. Gutiérrez-Martínez, J. Santos-Aguilar, R. Ochoa-Valiente, M. Santiago-Bernal, and A. Morales-Díaz, "Modeling and experimental electro-optic response of dielectric lithium niobate waveguides used as electric field sensors," *Meas. Sci. Technol.*, vol. 22, no. 3, pp. 035207-1–035207-7, Mar. 2011.

[24] P. J. Fish, *Electronic Noise and Low Noise Design*. New York, NY, USA: McGraw-Hilll, 1993, ch. 4.

[25] L. W. Couch, *Digital and Analog Communications Systems*. New York, NY, USA: Macmillan, 1993, ch. 2.

Celso Gutiérrez-Martínez (M'89) was born in Oaxaca, Mexico. He received the B.S. degree in electronics and communications engineering from ESIME, Instituto Politécnico Nacional, Mexico, in 1985, the M.S. degree in electrical engineering from CINVESTAV-IPN, in July 1985, and the Ph.D. degree in "sciences pour l'Ingenieur," from the Université de Franche-Comté, France, in 1994. Since November 1994, he has been with the Instituto Nacional de Astrofisica, Optica y Electronica, Tonantzintla, Mexico, where he works in the fields of electronics, optoelectronics, microwaves, millimeter waves, radio over fiber for telecommunications and signal processing.

Joel Santos-Aguilar was born in Puebla, México. He received the B.S. degree in electronics from the University of Puebla, Puebla, the M.Sc. degree in electronics and the Ph.D. degree in optics from the Instituto Nacional de Astrofisica, Optica y Electrónica, Tonantzintla, México, in 2005 and 2009, respectively. He is currently collaborating in research activities in optoelectronics and radio over fiber with the Centro de Invetigación Científica y Educación Superior de Ensenada, Ensenada, Mexico, in the frame of post-doctoral scholarship.

Adolfo Morales-Díaz was born in Puebla, México. He received the B.S. degree in electronics from the University of Puebla, Puebla, in June 2012. He is currently collaborating with the Instituto Nacional de Astrofisica, Optica y Electronica, Tonantzintla, México. He is currently on research activities related to radio-frequencies, optoelectronics and instrumentation.